

Coupled Tensor Completion via Low-rank Tensor Ring

Huyan Huang, Yipeng Liu, *Senior Member, IEEE*, Ce Zhu, *Fellow, IEEE*

Abstract—The coupled tensor decomposition aims to reveal the latent data structure which may share common factors. As a quantum inspired representation for tensors, the recently proposed tensor ring decomposition shows powerful representational ability. Using this decomposition, a novel non-convex model using the coupled tensor ring Frobenius norm is proposed in this paper. We also provide an excess risk bound for this model, which shows improvement compared with the recent coupled nuclear norm method. The model is solved by the block coordinate descent which only involves solving a series of quadratic forms constructed by the sampling pattern, thus it leads to efficient optimization. The proposed algorithm is validated on synthetic data and real-world data, which demonstrates the superiority over the existing coupled completion methods.

Index Terms—tensor ring, coupled tensor completion, alternating least squares, excess risk bound, permutational Rademacher complexity

I. INTRODUCTION

Tensor is a multi-dimensional array and able to model the interaction between different modes in high-dimensional data. Analogous to singular value decomposition (SVD), tensor decomposition seeks an optimal form of tensor representation which results in a set of smaller and simpler components. Tensor completion recovers the missing entries based on low-rank assumptions that are induced by different form of tensor decompositions. The completion methods are mainly divided into two categories. One is the convex method which is based on optimizing the low-rank inducing norms, the other one is the non-convex method which is based on optimizing the latent factors given pre-defined tensor rank. Tensor completion is applicable in many fields, such as signal processing [1]–[5], link prediction [6]–[8], recommendation system [9]–[14], bioinformatics [15]–[19], chemometrics [20], [21] and computer vision [22]–[31].

Sometimes the acquired data are not individual but share a part of information, and it can be regarded as a joint data where each individual provides the side information for the others. This may happen when several tensors share one or more dimensions, and we call them coupled tensors (see Figure 1). An advantage of modeling the data structure as coupled tensors is each tensor can obtain information from others and share information with others. The decomposition

for coupled tensors can be considered as a joint factorization, which simultaneously decomposes the tensors by sharing the low-rank property. The coupled tensor completion exploits the sharing low-rank structures to impute the missing entries in coupled tensors. Existing methods [32]–[35] for coupled tensor completion are based on CANDECOMP/PARAFAC (CP) decomposition, a generalization of SVD, which factorizes a D -order tensor into a linear combination of D rank-1 tensors, resulting in DIR parameters, provided that I is each dimensional size and R is the CP-rank.

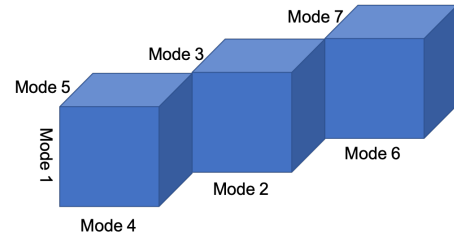


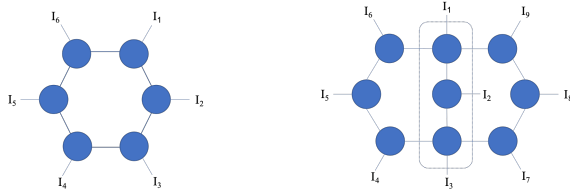
Fig. 1: Illustration of information sharing between three coupled tensors, through mode 1.

The recently proposed tensor ring (TR) decomposition represents a D -order tensor with cyclically contracted 3-order tensor factors of size $R \times I \times R$ by using the matrix product state expression (see Fig. 2(a)), resulting in DIR^2 parameters, where $[R, \dots, R]$ is the TR rank. The TR decomposition allows a cyclical shift of TR factors due to the nature of trace operator (see the detail in Section II-B), thus reordering tensor dimension makes no difference to the result. As a quantum inspired decomposition, the TR representation is shown to outperform CP and TK representations due to its powerful representation ability [31], [36], [37]. Though the TR rank is a vector, assuming all components has a same value is validated to be effective [37], which alleviates the burden of tuning many parameters.

In this paper, we focus on utilizing coupled TR decomposition for coupled tensor completion, and to the best of our knowledge, this is the first attempt to use TR decomposition for coupled tensor completion. The difference between the novelty of this paper and [37] is the derivation of closed form of sub-problems, which is crucial to the efficient optimization of the coupled TR factors. The proposed algorithm alternately solves a series of quadratic forms consisting of the latent factors. In optimization of the coupled TR factors, the value of its Hessian matrix is a mixture of the each individual Hessian matrix. The computation of each Hessian matrix depends on the sampling pattern, which may lead to a necessary

This research is supported by National Natural Science Foundation of China (NSFC, No. 61602091, No. 61571102) and the Sichuan Science and Technology program (No. 2019YFH0008, No.2018JY0035). The corresponding author is Yipeng Liu.

All the authors are with School of Information and Communication Engineering, University of Electronic Science and Technology of China (UESTC), Chengdu, 611731, China. (email: huyanhuang@gmail.com, yipengliu@uestc.edu.cn, cczhu@uestc.edu.cn).



(a) A graphical representation of the TR decomposition for a 6-order tensor. (b) A graphical representation of the coupled TR decomposition, where the first 3 modes are shared.

Fig. 2: Illustration of the coupled TR decomposition.

probabilistic condition for the sampling lower bound. We also analyze the computational and storage complexity. We then derive an excess risk bound using a recently proposed permutational Rademacher complexity, which shows that for coupled tensors, each can be recovered with a lower sampling rate that is below the sampling lower bound. The number of samples that can be reduced depends on the number of coupled dimensions. The proposed algorithm is evaluated on the synthetic data to verify the theory and compared with the coupled matrix-tensor factorization (CMFT) method [32]–[34] and the coupled nuclear norm (CNN) method [38] on real-world data to test its empirical performance. The result of numerical experiments show significant performance improvement in coupled data completion.

The remainder of this paper is arranged as follows. In Section II, we introduce basic notations and preliminaries of tensor, TR decomposition and its relevant operations. In Section III, we state the coupled TR completion problem and propose our algorithm, along with the algorithmic complexity. We also provide an excess risk bound for the coupled TR F-norm model. In Section IV, we perform a series of numerical experiments to compare the proposed method with the existing ones. Finally we conclude our work in Section V. The proof details of corresponding theories are shown in Appendix.

II. NOTATIONS AND PRELIMINARIES

A. Notations

Throughout the paper, a scalar, a vector, a matrix and a tensor are denoted by a normal letter, a boldfaced lower-case letter, a boldfaced upper-case letter and a calligraphic letter, respectively. For instance, a D -order tensor is denoted as $\mathcal{X} \in \mathbb{R}^{I_1 \times \dots \times I_D}$, where I_d is the dimensional size corresponding to mode- d , $d = 1, \dots, D$.

The Frobenius norm of \mathcal{X} is defined as the squared root of the inner product of twofold tensors:

$$\|\mathcal{X}\|_F = \sqrt{\langle \mathcal{X}, \mathcal{X} \rangle} = \sqrt{\sum_{i_1=1}^{I_1} \dots \sum_{i_D=1}^{I_D} x_{i_1 \dots i_D}^2}. \quad (1)$$

Projection operator $P_\Omega(\cdot)$ projects a tensor onto the support (observation) set Ω , where

$$\Omega := \{(i_1, \dots, i_D) \mid \text{if entry } (i_1, \dots, i_D) \text{ is observed}\} \quad (2)$$

For example, the formulation for a D -order tensor \mathcal{X} is

$$P_\Omega(\mathcal{X})_{i_1 \dots i_D} = \begin{cases} x_{i_1 \dots i_D} & (i_1, \dots, i_D) \in \Omega \\ 0 & (i_1, \dots, i_D) \notin \Omega \end{cases}. \quad (3)$$

The Hadamard product \otimes is an element-wise product. For D -order tensors \mathcal{X} and \mathcal{Y} , the representation is

$$(\mathcal{X} \otimes \mathcal{Y})_{i_1 \dots i_D} = x_{i_1 \dots i_D} \cdot y_{i_1 \dots i_D}. \quad (4)$$

The d -shifting K -unfolding yields a matrix $\mathbf{X}_{\{d, K\}} \in \mathbb{R}^{I_d \times J_d}$ by permuting \mathcal{X} with order $[d, \dots, D, 1, \dots, d-1]$ and unfolding along its first K dimensions, where $J_d = \prod_{n=1, n \neq d}^D I_n$.

B. Preliminaries of tensor ring decomposition

This section introduces the TR decomposition. Supposing the tensor \mathcal{X} has size $I_1 \times \dots \times I_D$. The non-canonical TR decomposition factorizes \mathcal{X} into D cyclically contracted 3-order tensors with the formulation [39]

$$\mathcal{X}(i_1, \dots, i_D) = \text{tr}(\mathcal{U}^{(1)}(:, i_1, :) \dots \mathcal{U}^{(D)}(:, i_D, :)), \quad (5)$$

where $\mathcal{U}^{(d)} \in \mathbb{R}^{R_d \times I_d \times R_{d+1}}$.

Reference [40] mentions two methods for TR decomposition. The first method is based on the density matrix renormalization group [41]. It firstly reshapes \mathcal{X} into $\mathbf{X}_{\{1,1\}}$ and applies SVD to derive $\mathbf{X}_{\{1,1\}} = \mathbf{U}\Sigma\mathbf{V}$. It then reshapes \mathbf{U} as the first TR factor and applies SVD to $\Sigma\mathbf{V}$. The algorithm is accomplished by performing $D-1$ SVDs. This method does not need the per-defined TR rank and performs fast. The second method alternatively optimizes one of the TR factors while keeping the others fixed. Repeatedly performing the optimization until the relative change $\|\mathcal{X}^k - \mathcal{X}^{k-1}\| / \|\mathcal{X}^{k-1}\|$ or the relative error $\|\mathcal{X}^k - \mathcal{X}_0\| / \|\mathcal{X}_0\|$ drops below a certain pre-defined threshold. This method requires a pre-defined TR rank which affects the performance and performs slowly compared with the first method.

III. COUPLED TENSOR RING COMPLETION ALGORITHM

We use \mathfrak{R} to represent the tensor ring computation (without any subscript) or itself (with subscript annotating the index) and assume the first L TR factors of \mathfrak{R}_1 and \mathfrak{R}_2 are coupled. Operator $\mathfrak{R}(\cdot)$ means the TR contraction which yields a tensor given a set of TR factors. Supposing $\{\mathcal{U}\} = \{\mathcal{U}^{(1)}, \dots, \mathcal{U}^{(D_1)}\}$ are the TR factors of \mathfrak{R}_1 , and $\{\mathcal{V}\} = \{\mathcal{V}^{(1)}, \dots, \mathcal{V}^{(D_2)}\}$ are the TR factors of \mathfrak{R}_2 . Assuming $\mathfrak{R}(\{\mathcal{U}\}) \in \mathbb{R}^{I_1 \times \dots \times I_{D_1}}$ and $\mathfrak{R}(\{\mathcal{V}\}) \in \mathbb{R}^{I'_1 \times \dots \times I'_{D_2}}$. Then the model for coupled TR completion is

$$\begin{aligned} & \min_{\{\mathcal{U}\}, \{\mathcal{V}\}} \frac{1}{2} \|\mathfrak{P}_{\Omega_1}(\mathfrak{R}(\{\mathcal{U}\})) - \mathfrak{P}_{\Omega_1}(\mathcal{T}_1)\|_2^2 + \\ & \frac{1}{2} \|\mathfrak{P}_{\Omega_2}(\mathfrak{R}(\{\mathcal{V}\})) - \mathfrak{P}_{\Omega_2}(\mathcal{T}_2)\|_2^2 \\ & \text{s. t. } \mathcal{U}^{(l)}(1 : \Gamma_l, :, 1 : \Gamma_{l+1}) = \mathcal{V}^{(l)}(1 : \Gamma_l, :, 1 : \Gamma_{l+1}) \\ & \quad l = 1, \dots, L, \end{aligned} \quad (6)$$

where $\Gamma_l \in [1, \min\{R_l, R'_l\}]$, $l = 1, \dots, L$ are the coupled distances, in which $[R_1, \dots, R_{D_1}]$ and $[R'_1, \dots, R'_{D_2}]$ are the TR ranks of $\mathfrak{R}(\{\mathcal{U}\})$ and $\mathfrak{R}(\{\mathcal{V}\})$, respectively.

At last, we emphasize that the coupled tensor ring model proposed in [42] is specific to the hyperspectral image super-resolution, which is different from ours in terms of model and algorithm.

A. Algorithm

To solve problem (6), we use the block coordinate descent method [43]. Specifically, this method alternately optimizes the block variable $\mathcal{U}^{(d_1)}$ (or $\mathcal{V}^{(d_2)}$) while keeping others fixed, thus the problem (6) is decomposed into $D_1 + D_2 - L$ sub-problems.

1) *Update of the uncoupled factors of \mathfrak{R}_1* : we rewrite problem (6) as

$$\min_{\mathcal{U}^{(d)}} \frac{1}{2} \|\mathbb{P}_{\Omega_1}(\mathfrak{R}(\{\mathcal{U}\})) - \mathbb{P}_{\Omega_1}(\mathcal{T}_1)\|_2^2 \quad (7)$$

and substitute $\mathcal{W}_1 \otimes (\cdot)$ for $\mathbb{P}_{\Omega_1}(\cdot)$. Let $\mathbf{A}_d \in \mathbb{R}^{I_d \times R_d R_{d+1}}$, $\mathbf{B}_d \in \mathbb{R}^{R_d R_{d+1} \times J_d}$ and $\mathbf{C}_d \in \mathbb{R}^{I_d \times J_d}$ be the unfoldings of $\mathcal{U}^{(d)}$, \mathcal{B}_d and \mathcal{T}_1 , respectively, where \mathcal{B}_d is computed by contracting all the D_1 TR factors of \mathfrak{R}_1 except the d -th factor. Then the problem (7) is converted into

$$\min_{\mathbf{A}_d, \mathbf{B}_d} \frac{1}{2} \|\mathbf{W}_{\{d,1\}} \otimes \mathbf{A}_d \mathbf{B}_d - \mathbf{W}_{1\{d,1\}} \otimes \mathbf{C}_d\|_{\mathbb{F}}^2 \quad (8)$$

Defining $\mathbf{w}_{i_d}^{(d)} = \mathbf{W}_{\{d,1\}}(i_d, :)$ and a permutation matrix $\mathbf{P}_{i_d}^{(d)} \in \mathbb{R}^{I_d \times I_d}$ where \mathbf{e}_k is a vector of length I_d with k -th entry, $k \in \mathbb{S}_{i_d}^{(d)}$ and $\mathbb{S}_{i_d}^{(d)} = \{j_d | \mathbf{w}_{i_d}^{(d)}(j_d) = 1\}$.

Note that the d -th sub-problem in (8) can be divided into I_d sub-sub-problems, in which the row vectors $\mathbf{a}_{i_d}^{(d)} = \mathbf{A}_d(i_d, :)$ are treated as the block variables. Reformulating the i_d -th sub-sub-problem in the quadratic form and calculating its first-order derivative, we have the optimal solution of the form

$$\mathbf{a}_{i_d}^{(d)*} = -\mathbf{g}_{i_d}^{(d)} \mathbf{H}_{i_d}^{(d)\dagger}, \quad (9)$$

where \dagger is the Moore-Penrose pseudoinverse and

$$\begin{cases} \mathbf{H}_{i_d}^{(d)} = \overline{\mathbf{B}}_{i_d}^{(d)} \overline{\mathbf{B}}_{i_d}^{(d)\top}, & \mathbf{g}_{i_d}^{(d)} = -\overline{\mathbf{c}}_{i_d}^{(d)} \overline{\mathbf{B}}_{i_d}^{(d)\top} \\ \overline{\mathbf{c}}_{i_d}^{(d)} = \mathbf{c}_{i_d}^{(d)} \mathbf{P}_{i_d}^{(d)}, & \overline{\mathbf{B}}_{i_d}^{(d)} = \mathbf{B}_{i_d}^{(d)} \mathbf{P}_{i_d}^{(d)} \end{cases}.$$

The TR factor $\mathcal{U}^{(d)}$ is optimized by performing (9) I_d times to solve the d -th sub-problem of (8). Then the uncoupled TR factors of \mathfrak{R}_1 are updated by optimizing all $D_1 - L$ factors.

2) *Update of the uncoupled factors of \mathfrak{R}_2* : This optimization is similar to the update of uncoupled TR factors of \mathfrak{R}_1 and can refer to (9), hence we skip the deduction and just give the solution as

$$\mathbf{a}'_{i'_d}{}^{(d)*} = \mathbf{g}'_{i'_d}{}^{(d)} \mathbf{H}'_{i'_d}{}^{(d)\dagger}, \quad (10)$$

where $\mathbf{H}'_{i'_d}{}^{(d)} = \overline{\mathbf{B}}'_{i'_d}{}^{(d)} \overline{\mathbf{B}}'_{i'_d}{}^{(d)\top}$, $\mathbf{g}'_{i'_d}{}^{(d)} = -\overline{\mathbf{c}}'_{i'_d}{}^{(d)} \mathbf{B}'_{i'_d}{}^{(d)\top}$, $\mathbf{z}'_{i'_d}{}^{(d)} = \overline{\mathbf{c}}'_{i'_d}{}^{(d)} \mathbf{c}'_{i'_d}{}^{(d)}$, and the symbols with superscript $'$ means the corresponding terms derived from computation of \mathfrak{R}_2 .

3) *Update of the coupled factors of \mathfrak{R}_1 and \mathfrak{R}_2* : we rewrite the problem (6) as

$$\begin{aligned} & \min_{\substack{\mathcal{U}^{(d)}, \mathcal{V}^{(d)} \\ d=1, \dots, L}} \frac{1}{2} \|\mathbb{P}_{\Omega_1}(\mathfrak{R}(\{\mathcal{U}\})) - \mathbb{P}_{\Omega_1}(\mathcal{T}_1)\|_2^2 + \\ & \frac{1}{2} \|\mathbb{P}_{\Omega_2}(\mathfrak{R}(\{\mathcal{V}\})) - \mathbb{P}_{\Omega_2}(\mathcal{T}_2)\|_2^2 \quad (11) \\ \text{s. t. } & \mathcal{U}^{(d)}(1 : \Gamma_d, :, 1 : \Gamma_{d+1}) = \\ & \mathcal{V}^{(d)}(1 : \Gamma_d, :, 1 : \Gamma_{d+1}), \quad d = 1, \dots, L. \end{aligned}$$

Let $\mathbf{A}'_d \in \mathbb{R}^{I'_d \times R_d R_{d+1}}$ be the unfolding of $\mathcal{V}^{(d)}$, $\mathbf{C}'_d \in \mathbb{R}^{I'_d \times J'_d}$ be the $\{d, 1\}$ unfolding of \mathcal{T}_2 and \mathcal{W}' be the tensor form of \mathbb{P}_{Ω_2} . Let

$$\begin{aligned} \mathbb{C}_d &= \{1, \dots, \Gamma_{d+1}, R_{d+1} + 1, \dots, R_{d+1} + \Gamma_{d+1}, \\ & \dots, \\ & \Gamma_d R_{d+1} + 1, \dots, \Gamma_d R_{d+1} + \Gamma_{d+1}\}, \quad d = 1, \dots, L, \\ \mathbb{C}'_d &= \{1, \dots, \Gamma_{d+1}, R'_{d+1} + 1, \dots, R'_{d+1} + \Gamma_{d+1}, \\ & \dots, \\ & \Gamma_d R'_{d+1} + 1, \dots, \Gamma_d R'_{d+1} + \Gamma_{d+1}\}, \quad d = 1, \dots, L. \end{aligned}$$

We reformulate (11) as

$$\begin{aligned} & \min_{\substack{\mathbf{A}_d, \mathbf{A}'_d \\ d=1, \dots, L}} \frac{1}{2} \|\mathbf{W}_{\{d,1\}} \otimes \mathbf{A}_d \mathbf{B}_d - \mathbf{W}_{\{d,1\}} \otimes \mathbf{C}_d\|_{\mathbb{F}}^2 + \\ & \frac{1}{2} \|\mathbf{W}'_{\{d,1\}} \otimes \mathbf{A}'_d \mathbf{B}'_d - \mathbf{W}'_{\{d,1\}} \otimes \mathbf{C}'_d\|_{\mathbb{F}}^2 \quad (12) \\ \text{s. t. } & \mathbf{A}_d(:, \mathbb{C}_d) = \mathbf{A}'_d(:, \mathbb{C}'_d), \quad d = 1, \dots, L, \end{aligned}$$

where the index sets $\mathbb{C}_d \in \mathbb{R}^{\Gamma_d \Gamma_{d+1}}$ and $\mathbb{C}'_d \in \mathbb{R}^{\Gamma_d \Gamma_{d+1}}$ indicate which columns are coupled in \mathbf{A}_d and \mathbf{A}'_d , respectively.

Following the analysis in optimization (8), we consider the i_d -th sub-sub-problem of the d -th sub-problem of (12). Defining

$$\begin{cases} \boldsymbol{\alpha}_{i_d}^{(d)} \triangleq \mathbf{A}_d(i_d, \mathbb{C}_d) = \mathbf{A}'_d(i_d, \mathbb{C}'_d) \\ \boldsymbol{\beta}_{i_d}^{(d)} \triangleq \mathbf{A}_d(i_d, \{1, \dots, R_d R_{d+1}\} \setminus \mathbb{C}_d) \\ \boldsymbol{\gamma}_{i_d}^{(d)} \triangleq \mathbf{A}'_d(i_d, \{1, \dots, R'_d R'_{d+1}\} \setminus \mathbb{C}'_d) \end{cases},$$

then $\mathbf{A}_d(i_d, :)$ and $\mathbf{A}'_d(i_d, :)$ are $[\boldsymbol{\alpha}_{i_d}^{(d)}, \boldsymbol{\beta}_{i_d}^{(d)}] \mathbf{P}_d^{\top}$ and $[\boldsymbol{\alpha}_{i_d}^{(d)}, \boldsymbol{\gamma}_{i_d}^{(d)}] \mathbf{P}'_d{}^{\top}$, where $\mathbf{P}_d = [\mathbf{e}_{\mathbb{C}_d}, \mathbf{e}_{\{1, \dots, R_d R_{d+1}\} \setminus \mathbb{C}_d}]$ and $\mathbf{P}'_d = [\mathbf{e}_{\mathbb{C}'_d}, \mathbf{e}_{\{1, \dots, R'_d R'_{d+1}\} \setminus \mathbb{C}'_d}]$ are permutation matrices. Accordingly, we have the problem

$$\begin{aligned} & \min_{\boldsymbol{\alpha}_{i_d}^{(d)}, \boldsymbol{\beta}_{i_d}^{(d)}, \boldsymbol{\gamma}_{i_d}^{(d)}} \frac{1}{2} \|\mathbf{w}_{i_d}^{(d)} \otimes [\boldsymbol{\alpha}_{i_d}^{(d)}, \boldsymbol{\beta}_{i_d}^{(d)}] \mathbf{P}_d^{\top} \mathbf{B}_d - \mathbf{w}_{i_d}^{(d)} \otimes \mathbf{c}_{i_d}^{(d)}\|_2^2 \\ & + \frac{1}{2} \|\mathbf{w}'_{i_d}{}^{(d)} \otimes [\boldsymbol{\alpha}_{i_d}^{(d)}, \boldsymbol{\gamma}_{i_d}^{(d)}] \mathbf{P}'_d{}^{\top} \mathbf{B}'_d - \mathbf{w}'_{i_d}{}^{(d)} \otimes \mathbf{c}'_{i_d}{}^{(d)}\|_2^2. \quad (13) \end{aligned}$$

Let $\widetilde{\mathbf{H}}_{i_d}^{(d)} = \mathbf{P}_d^{\top} \mathbf{H}_{i_d}^{(d)} \mathbf{P}_d$ and $\widetilde{\mathbf{H}}'_{i_d}{}^{(d)} = \mathbf{P}'_d{}^{\top} \mathbf{H}'_{i_d}{}^{(d)} \mathbf{P}'_d$. Defining

$$\widetilde{\mathbf{H}}_{i_d}^{(d)} \triangleq \begin{bmatrix} \widetilde{\mathbf{H}}_{i_d}^{(d)11} & \widetilde{\mathbf{H}}_{i_d}^{(d)12} \\ \widetilde{\mathbf{H}}_{i_d}^{(d)21} & \widetilde{\mathbf{H}}_{i_d}^{(d)22} \end{bmatrix}, \quad \widetilde{\mathbf{H}}'_{i_d}{}^{(d)} \triangleq \begin{bmatrix} \widetilde{\mathbf{H}}'_{i_d}{}^{(d)11} & \widetilde{\mathbf{H}}'_{i_d}{}^{(d)12} \\ \widetilde{\mathbf{H}}'_{i_d}{}^{(d)21} & \widetilde{\mathbf{H}}'_{i_d}{}^{(d)22} \end{bmatrix},$$

such that

$$\begin{aligned}\widetilde{\mathbf{H}}_{i_d}^{(d)11} &\in \mathbb{R}^{\Gamma_d \Gamma_{d+1} \times \Gamma_d \Gamma_{d+1}}, \\ \widetilde{\mathbf{H}}_{i_d}^{(d)12} &\in \mathbb{R}^{\Gamma_d \Gamma_{d+1} \times R_d R_{d+1} - \Gamma_d \Gamma_{d+1}}, \\ \widetilde{\mathbf{H}}_{i_d}^{(d)21} &\in \mathbb{R}^{R_d R_{d+1} - \Gamma_d \Gamma_{d+1} \times \Gamma_d \Gamma_{d+1}}, \\ \widetilde{\mathbf{H}}_{i_d}^{(d)22} &\in \mathbb{R}^{R_d R_{d+1} - \Gamma_d \Gamma_{d+1} \times R_d R_{d+1} - \Gamma_d \Gamma_{d+1}}\end{aligned}$$

and the similar sizes hold for $\widetilde{\mathbf{H}}_{i_d}^{(d)11}$, $\widetilde{\mathbf{H}}_{i_d}^{(d)12}$, $\widetilde{\mathbf{H}}_{i_d}^{(d)21}$ and $\widetilde{\mathbf{H}}_{i_d}^{(d)22}$. Defining

$$\begin{cases} \mathbf{g}_{i_d}^{(d)} \triangleq -\widetilde{\mathbf{c}}_{i_d}^{(d)} \widetilde{\mathbf{B}}_{i_d}^{(d)\top} \mathbf{P}_d = [\boldsymbol{\xi}_{i_d}^{(d)}, \boldsymbol{\eta}_{i_d}^{(d)}] \\ \mathbf{g}'_{i_d}^{(d)} \triangleq -\widetilde{\mathbf{c}}'_{i_d}{}^{(d)} \widetilde{\mathbf{B}}'_{i_d}{}^{(d)\top} \mathbf{P}'_d = [\boldsymbol{\xi}'_{i_d}{}^{(d)}, \boldsymbol{\eta}'_{i_d}{}^{(d)}] \end{cases}$$

such that $\boldsymbol{\xi}_{i_d}^{(d)}, \boldsymbol{\xi}'_{i_d}{}^{(d)} \in \mathbb{R}^{\Gamma_d \Gamma_{d+1}}$, $\boldsymbol{\eta}_{i_d}^{(d)} \in \mathbb{R}^{R_d R_{d+1} - \Gamma_d \Gamma_{d+1}}$ and $\boldsymbol{\eta}'_{i_d}{}^{(d)} \in \mathbb{R}^{R_d R_{d+1} - \Gamma_d \Gamma_{d+1}}$.

We then deduce the solution (see Appendix A for detail) as

$$\begin{aligned}& [\boldsymbol{\alpha}_{i_d}^{(d)}, \boldsymbol{\beta}_{i_d}^{(d)}, \boldsymbol{\gamma}_{i_d}^{(d)}]^* \\ &= \arg \min_{\substack{\boldsymbol{\alpha}_{i_d}^{(d)}, \boldsymbol{\beta}_{i_d}^{(d)} \\ \boldsymbol{\gamma}_{i_d}^{(d)}}} \frac{1}{2} [\boldsymbol{\alpha}_{i_d}^{(d)}, \boldsymbol{\beta}_{i_d}^{(d)}, \boldsymbol{\gamma}_{i_d}^{(d)}] \widehat{\mathbf{H}}_{i_d}^{(d)} [\boldsymbol{\alpha}_{i_d}^{(d)}, \boldsymbol{\beta}_{i_d}^{(d)}, \boldsymbol{\gamma}_{i_d}^{(d)}]^\top \\ &+ [\boldsymbol{\alpha}_{i_d}^{(d)}, \boldsymbol{\beta}_{i_d}^{(d)}, \boldsymbol{\gamma}_{i_d}^{(d)}] [\boldsymbol{\xi}_{i_d}^{(d)} + \boldsymbol{\xi}'_{i_d}{}^{(d)}, \boldsymbol{\eta}_{i_d}^{(d)}, \boldsymbol{\eta}'_{i_d}{}^{(d)}]^\top + \\ &\frac{1}{2} z_{i_d}^{(d)} + \frac{1}{2} z'_{i_d}{}^{(d)} \\ &= -\widehat{\mathbf{g}}_{i_d}^{(d)} \widehat{\mathbf{H}}_{i_d}^{(d)\dagger},\end{aligned}\quad (14)$$

where $\widehat{\mathbf{g}}_{i_d}^{(d)} = [\boldsymbol{\xi}_{i_d}^{(d)} + \boldsymbol{\xi}'_{i_d}{}^{(d)}, \boldsymbol{\eta}_{i_d}^{(d)}, \boldsymbol{\eta}'_{i_d}{}^{(d)}]$ and the Hessian matrix is

$$\widehat{\mathbf{H}}_{i_d}^{(d)} = \begin{bmatrix} \widetilde{\mathbf{H}}_{i_d}^{(d)11} + \widetilde{\mathbf{H}}_{i_d}^{\prime(d)11} & \widetilde{\mathbf{H}}_{i_d}^{(d)12} + \widetilde{\mathbf{H}}_{i_d}^{\prime(d)12} & \widetilde{\mathbf{H}}_{i_d}^{(d)12} + \widetilde{\mathbf{H}}_{i_d}^{\prime(d)21\top} \\ \widetilde{\mathbf{H}}_{i_d}^{(d)21} + \widetilde{\mathbf{H}}_{i_d}^{\prime(d)12\top} & \widetilde{\mathbf{H}}_{i_d}^{(d)22} & \mathbf{0} \\ \widetilde{\mathbf{H}}_{i_d}^{\prime(d)21} + \widetilde{\mathbf{H}}_{i_d}^{\prime(d)12\top} & \mathbf{0} & \widetilde{\mathbf{H}}_{i_d}^{\prime(d)22} \end{bmatrix}$$

The algorithm for coupled tensor completion via low-rank tensor ring is outlined in Algorithm 1.

Note this algorithm can be easily extend to the case where more than two tensor rings are coupled, in which only the scheme for updating the coupled components is changed. We have the Hessian matrix defined in the form of block matrix

$$\begin{cases} \widehat{\mathbf{H}}_{i_d}^{(d)} \{1, 1\} = \sum_{n=1}^N \widehat{\mathbf{H}}_{i_d}^{(n)} \{1, 1\}, \widehat{\mathbf{H}}_{i_d} \{n, n\} = \widehat{\mathbf{H}}_{i_d}^{(n)} \{1, 1\} \\ (n = 2, \dots, N), \\ \widehat{\mathbf{H}}_{i_d}^{(d)} \{1, n\} = \widehat{\mathbf{H}}_{i_d} \{n, 1\}^\top = \widehat{\mathbf{H}}_{i_d}^{(n)} \{1, 1\} + \widehat{\mathbf{H}}_{i_d}^{(n)} \{d, 21\}^\top \\ (n = 2, \dots, N), \\ \widehat{\mathbf{H}}_{i_d}^{(d)} \{m, n\} = \mathbf{0} \quad (m \neq n, m \neq 1, n \neq 1) \end{cases}$$

and $\widehat{\mathbf{g}}_{i_d}^{(d)} = [\sum_{n=1}^N \boldsymbol{\xi}_{i_d}^{(n)}, \boldsymbol{\eta}_{i_d}^{(d)}, \boldsymbol{\eta}_{i_d}^{(N)}]^\top$, where $\widehat{\mathbf{H}}_{i_d}^{(n)} \{1, 1\} =$

Algorithm 1 Alternating least squares for coupled tensor ring completion (CTRC)

Input: Two zero-filled tensors \mathcal{T}_1 and \mathcal{T}_2 , two binary tensors \mathcal{W}_1 and \mathcal{W}_2 , the maximal # iterations K

Output: Two recovered tensors \mathcal{X} and \mathcal{Y} , two sets of TR factors $\{\mathcal{U}\}$ and $\{\mathcal{V}\}$

- 1: Apply Algorithm 1 to initialize $\{\mathcal{U}\}$ and $\{\mathcal{V}\}$
- 2: **for** $k = 1$ **to** K **do**
- 3: Update the uncoupled TR factors of \mathfrak{R}_1 according to (9)
- 4: Update the uncoupled TR factors of \mathfrak{R}_2 according to (10)
- 5: Update the coupled TR factors of \mathfrak{R}_1 and \mathfrak{R}_2 according to (14)
- 6: Update $\mathcal{X} = \mathfrak{R}(\{\mathcal{U}\})$, $\mathcal{Y} = \mathfrak{R}(\{\mathcal{V}\})$
- 7: **if** converged **then**
- 8: break
- 9: **end if**
- 10: **end for**
- 11: **return** $\mathcal{X}, \mathcal{Y}, \{\mathcal{U}\}, \{\mathcal{V}\}$

$\mathbf{P}_d^{(n)\top} \mathbf{H}_{i_d}^{(n)} \mathbf{P}_d^{(n)}$ and

$$\widetilde{\mathbf{g}}_{i_d}^{(n)} \triangleq -\widetilde{\mathbf{c}}_{i_d}^{(n)} \widetilde{\mathbf{B}}_d^{(n)\top} \mathbf{P}_d^{(n)} = [\boldsymbol{\xi}_{i_d}^{(n)}, \boldsymbol{\eta}_{i_d}^{(n)}]^\top.$$

B. Computational Complexity

Assuming all the tensors $\mathcal{X}_1, \dots, \mathcal{X}_N$ have a same size $I_1 \times \dots \times I_D$ and a same TR rank $[R, \dots, R]$. The computation of Hessian matrix $\mathbf{H}_{i_d}^{(d)}$ costs $O(\text{SR} \times R^4 \prod_{k=1, k \neq d}^D I_k) = O(mR^4/I_d)$, where SR is the sampling rate. Thus updating the d -th TR factor costs $O(mR^4)$ and one iteration of CTRC costs $O(mNDR^4)$.

The computation of $\mathbf{H}_{i_d}^{(d)\dagger}$ costs $O(R^6)$ and updating the d -th TR factor costs $O(I_d R^6)$. Hence one iteration of CTRC costs $O(NR^6 \sum_{d=1}^D I_d)$.

The total computational cost of one iteration of CTRC is $\max\{O(mNDR^4), O(NR^6 \sum_{d=1}^D I_d)\} = O(mNDR^4)$.

C. Excess Risk Bound

We define $\bar{l}_{\mathbb{T}}(\cdot, \cdot)$ as the average of the perfect square trinomial $l(\cdot, \cdot)$ computed on a finite training set \mathbb{T} . For concise expression of average test error, we use notation $\bar{l}_{\mathbb{T}}(\{\mathcal{X}, \mathcal{Y}\}, \{\mathcal{T}_1, \mathcal{T}_2\})$ to denote the average training error over \mathbb{T} , where we simply refer to $\mathbb{T} \subseteq \Omega$ as the union of $\mathbb{T}_1 \subseteq \Omega_1$ and $\mathbb{T}_2 \subseteq \Omega_2$. Similarly, we can define $\bar{l}_{\mathbb{S}}(\mathcal{X}, \mathcal{Y})$ as the average test error measured by $l(\cdot, \cdot)$ over $\mathbb{S} \subseteq \Omega^\perp$. As in [44], we assume that $|\mathbb{S}_i| = |\mathbb{T}_i|$ for any $i \in \{1, 2\}$.

Given an assumption that $\mathcal{X} = \mathfrak{R}(\{\mathcal{U}\})$ with TR rank $[R, \dots, R]$ and each TR factor is a independent Gaussian random tensor with zero mean and variance of σ^2 , we can define a hypothesis class $\mathcal{H} \triangleq \{\mathcal{X}, \mathcal{Y} \mid \mathcal{U}^{(d)} \sim \mathcal{N}(0, \sigma^2), \mathcal{V}^{(d)} \sim \mathcal{N}(0, \sigma^2)\}$. Without loss of generality, we assume $l(\cdot, \cdot)$ is L -Lipschitz continuous since

the F-norms of two tensors are centralized with overwhelming probability.

By leveraging the recently proposed permutational Rademacher complexity [44], the following theorem characterizes the excess risk of coupled TR completion.

Theorem 1. *Under the hypothesis \mathcal{H} mentioned before, the excess risk of the coupled TR completion (6) is bounded as*

$$\begin{aligned} & \bar{l}_{\mathbb{S}}(\{\mathcal{X}, \mathcal{Y}\}, \{\mathcal{T}_1, \mathcal{T}_2\}) - \bar{l}_{\mathbb{T}}(\{\mathcal{X}, \mathcal{Y}\}, \{\mathcal{T}_1, \mathcal{T}_2\}) \leq \\ & \Lambda \left(1 + \frac{2}{\sqrt{2\pi|\mathbb{T}|-2}} \right) \frac{(2\sigma)^{\frac{D_1}{2}} \Gamma^{D_1} \left(\frac{IR^2+1}{2} \right)}{\sqrt{|\mathbb{T}_1|} \Gamma^{D_1} \left(\frac{IR^2}{2} \right)} \\ & {}_{D_2+1-L}F_{D_1-L} \left(\begin{matrix} -\frac{1}{2}, \frac{IR^2}{2}, \dots, \frac{IR^2}{2} \\ 1-IR^2, \dots, 1-IR^2 \end{matrix} \middle| (-1)^{D_1+1-L} \frac{|\mathbb{T}_1| (2\sigma)^{D_2}}{|\mathbb{T}_2| (2\sigma)^{D_1}} \right) + \\ & \sqrt{\frac{2|\mathbb{T} \cup \mathbb{S}| \ln(1/\delta)}{(|\mathbb{T} \cup \mathbb{S}| - 1/2)^2}} \end{aligned} \quad (15)$$

for $D_1 \geq D_2$ and

$$\begin{aligned} & \bar{l}_{\mathbb{S}}(\{\mathcal{X}, \mathcal{Y}\}, \{\mathcal{T}_1, \mathcal{T}_2\}) - \bar{l}_{\mathbb{T}}(\{\mathcal{X}, \mathcal{Y}\}, \{\mathcal{T}_1, \mathcal{T}_2\}) \leq \\ & \Lambda \left(1 + \frac{2}{\sqrt{2\pi|\mathbb{T}|-2}} \right) \frac{\sigma^{D_2} 2^{\frac{D_2}{2}} \Gamma^{D_2} \left(\frac{IR^2+1}{2} \right)}{\sqrt{|\mathbb{T}_2|} \Gamma^{D_2} \left(\frac{IR^2}{2} \right)} \\ & {}_{D_1+1-L}F_{D_2-L} \left(\begin{matrix} -\frac{1}{2}, \frac{IR^2}{2}, \dots, \frac{IR^2}{2} \\ 1-IR^2, \dots, 1-IR^2 \end{matrix} \middle| (-1)^{D_2+1-L} \frac{|\mathbb{T}_2| (2\sigma)^{D_1}}{|\mathbb{T}_1| (2\sigma)^{D_2}} \right) + \\ & \sqrt{\frac{2|\mathbb{T} \cup \mathbb{S}| \ln(1/\delta)}{(|\mathbb{T} \cup \mathbb{S}| - 1/2)^2}} \end{aligned} \quad (16)$$

for $D_2 \geq D_1$ respectively with probability at least $1 - \delta$. Moreover, with the same probability, the excess risk of each individual TR completion is bounded by

$$\begin{aligned} & \Lambda \left(1 + \frac{2}{\sqrt{2\pi|\mathbb{T}_n|-2}} \right) \frac{(2\sigma)^{\frac{D_n}{2}} \Gamma^{D_n} \left(\frac{IR^2+1}{2} \right)}{\sqrt{|\mathbb{T}_n|} \Gamma^{D_n} \left(\frac{IR^2}{2} \right)} + \\ & \sqrt{\frac{2|\mathbb{T}_n \cup \mathbb{S}_n| \ln(1/\delta)}{(|\mathbb{T}_n \cup \mathbb{S}_n| - 1/2)^2}}, \quad n = 1, 2. \end{aligned} \quad (17)$$

Theorem 1 reports a phenomenon that the risk bound of coupled completion can be much lower than that of individual completion. Notice that these expressions are multiplicative, it suffices to illustrate the relationship by comparing each term. The term $\sqrt{|\mathbb{T}|}$ in the denominator is larger than each single part. Note that the hypergeometric function approximates to 1 if the input argument approximates to 0. Supposing that $D_1 \geq D_2$ without loss of generality, then this function can yield a number close to 1 by choosing $|\mathbb{T}_1|$ and $|\mathbb{T}_2|$ such that $|\mathbb{T}_1|$ is enough less than $|\mathbb{T}_2|$. Thus the risk bound (15) or (16) is less than the sum of the bounds (17).

To discuss the effect of these parameters on the risk bound, note that $\mathbb{E} \left[\sqrt{X} \right] \leq \sqrt{\mathbb{E}[X]}$, a supremum of the risk bound

(follows from Appendix B) is given by

$$\begin{aligned} & \Lambda \left(1 + \frac{2}{\sqrt{2\pi|\mathbb{T}|-2}} \right) \\ & (2\sigma)^{\frac{D_n}{2}} \frac{\Gamma^L \left(\frac{IR^2+1}{2} \right)}{\Gamma^L \left(\frac{IR^2}{2} \right)} \sqrt{\frac{(\sigma IR^2)^{D_1-L}}{|\mathbb{T}_1|} + \frac{(\sigma IR^2)^{D_2-L}}{|\mathbb{T}_1|}}. \end{aligned}$$

Therefore increasing $|\mathbb{T}_1|$ or $|\mathbb{T}_2|$ or both are beneficial to the recovery performance, but the increments of I , R , D_1 and D_2 are unfavorable. To examine the effect of L , let $f(L)$ be the above term, then

$$f'(L) = \frac{1}{2} f(L) \left[\ln \left(2 \frac{\Gamma^2 \left(\frac{k+1}{2} \right)}{\Gamma^2 \left(\frac{k}{2} \right)} \right) - \ln(k) \right],$$

where $k = IR^2$. Since for a Chi distributed variable X with degree of freedom k we have $\mathbb{E}^2[X] \leq \mathbb{E}[X^2]$, and hence $f'(L) < 0$. This means increasing the number of coupled dimensions improves the recovery performance.

This coupled completion can also be comprehended from the viewpoint of mutual information $I(\mathcal{X}; \mathcal{Y}) = \iint p(\mathcal{X}, \mathcal{Y}) \ln \frac{p(\mathcal{X}, \mathcal{Y})}{p(\mathcal{X})p(\mathcal{Y})} d\mathcal{X}d\mathcal{Y}$. The two tensor rings have no mutual information if they are not coupled, thus they cannot help each other's recovery. On the other hand, this term becomes the differential entropy $H(\mathcal{X})$ if they are totally coupled, meanwhile, the amount of information reaches the maximum which results in the best recovery performance. The information transfer consists in the summation of the Hessian matrices in Algorithm 1 since the amplitude ratio of the matrices is $|\mathbb{T}_1|/|\mathbb{T}_2|$.

As a comparison, the bound of our coupled F-norm is on the order of $I^{D/2}$ which is lower than the bound in [38], i.e., $O \left(I^{(D+1)/2} \ln^{D-1/2}(I) \right)$ by considering bounding the nuclear norm of the coupled tensor.

IV. NUMERICAL EXPERIMENT

In this section, the proposed algorithm is evaluated on two kinds of datasets, i.e., synthetic data and real-world data. The synthetic data is employed to verify the theory. To test the empirical performance of the proposed CTRC, the CTRC along with other three algorithms are benchmarked on real-world data, including the coupled nuclear norm minimization for coupled tensor completion (CNN) [38], advanced coupled matrix and tensor factorization (ACMTF) [33], [34] structured data fusion by nonlinear least squares (SDF) [35]. The low rank tensor completion via alternating least square (TR-ALS) [37] is also compared as a baseline since it can be regarded as the individual tensor ring completion.

The root of mean square error (RMSE) defined as $\text{RMSE} = \|\hat{\mathcal{X}} - \mathcal{X}\|_{\text{F}} / \sqrt{|\mathcal{X}|}$ is used as the completion score, where \mathcal{X} is the ground truth and $\hat{\mathcal{X}}$ is the estimate of \mathcal{X} . We use computational CPU time (in seconds) as a measure of algorithmic complexity.

The sampling rate (SR) is defined as the ratio of the number of samples to the total number of the elements of tensor \mathcal{X} , which is denoted as $\text{SR} = |\Omega|/|\mathcal{X}|$. For fair comparison, the parameters in each algorithm are tuned to give optimal perfor-

mance. For the proposed CTTC algorithm, one of the stop criteria is that the relative change $RC = \|\mathcal{X}_k - \mathcal{X}_{k-1}\|_F / \|\mathcal{X}_{k-1}\|_F$ is less than a tolerance that is set to 1×10^{-8} . We set the maximal number of iterations $K = 200$ in experiments on synthetic data and $K = 100$ in experiments on real-world data.

All the experiments are conducted in MATLAB 9.7.0 on a computer with a 2.8GHz CPU of Intel Core i7 and a 16GB RAM.

A. Synthetic Data

In this section, we test our algorithm on randomly generated completion problem. We generate two tensors of the same size $20 \times 20 \times 20 \times 20$ using the TR decomposition (5), in which the TR factors are randomly sampled from the standard normal distribution, i.e., $\mathcal{U}^{(d)}(r_d, i_d, r_{d+1}) \sim \mathcal{N}(0, 1)$, $\mathcal{V}^{(d)}(r_d, i_d, r_{d+1}) \sim \mathcal{N}(0, 1)$, $d = 1, \dots, 4$. Then we couple two tensor rings by setting $\mathcal{U}^{(d)} = \mathcal{V}^{(d)}$, $d = 1, \dots, 3$. Next, we compute the tensors \mathcal{T}_1 and \mathcal{T}_2 according to these factors. We run our algorithm to plot the phase transition on TR rank versus sampling rate of tensor \mathcal{T}_1 under different settings of sampling rate of tensor \mathcal{T}_2 and the number of coupled TR factors. The sampling rate of \mathcal{T}_1 ranges from 0.005 to 0.1 with interval 0.005, and the sampling rate of \mathcal{T}_2 ranges from 0.05 to 0.2 with interval 0.05. The TR rank varies from 2 to 8, and the number of coupled TR factors is 1, 2 and 3.

Fig. 3 reports the result. The Dim_c in the figure represents the number of the coupled TR factors, and SR_1 and SR_2 represent the sampling rates of \mathcal{T}_1 and \mathcal{T}_2 , respectively. In phase transition, the white patch means a successful recovery whose RMSE is less than 1×10^{-6} , and the black patch means a failure. The successful area increases when sampling rate of \mathcal{T}_2 or the number of the coupled TR factors increases. This is because the first tensor ring can learn information from the second one with increasing sampling rate or the number of coupled factors, though the recovery of \mathcal{T}_1 is beyond its sampling limit. Numerically, the magnitude of the singular values of Hessian matrix $\tilde{\mathbf{H}}'_{i_d}$ is SR_2/SR_1 times the magnitude of the singular values of $\tilde{\mathbf{H}}_{i_d}$, hence the $\tilde{\mathbf{H}}'_{i_d}$ is dominated in the updating scheme.

B. The UCLAF Data

In this section, the user-centered collaborative location and activity filtering (UCLAF) data [45] is used for benchmark. It comprises 164 users' GPS trajectories based on their partial 168 locations and 5 activity annotations. In the experiment, we only use the link activity, i.e., only entry greater than 0 is set to 1. Then we remove users with no data, which results in a sparse tensor of size $144 \times 168 \times 5$. The user-location matrix which has size 144×168 is coupled with this tensor as a side information. We randomly pick 50% samples from the tensor and the matrix independently. For each algorithm we conduct 10 experiments for avoiding fortuitous result.

Fig. 4 shows the average completion result versus tensor rank derived by five algorithms, in which the completion score is measured by RMSE. The label "TR" means the individual

tensor ring completion method which is a baseline for comparing with the coupled tensor ring completion method. From the result, the coupled completion method performs better than the individual one. The proposed CTTC shows lower RMSEs in both user-loc-act tensor completion and user-loc matrix completion, which illustrates that the coupled TR's F-norm can lead to better performance compared with other coupled norms.

C. The SW-NIR Data

A dataset consists of a set of short-wave near-infrared (SW-NIR) spectrum [46] measured on an HP diode array spectrometer is used in this section's experiment. It is used to trace the influence of the temperature on vibrational spectrum and the consequences for the predictive ability of multivariate calibration models. The spectrum of 19 mixtures of ethanol, water and isopropanol and the spectrum of the pure compounds are recorded in a 1 cm cuvette at different temperatures, i.e., 30, 40, 50, 60 and 70 degrees Celsius. We stack each spectrum recorded at different temperatures in the third dimension and forms a tensor of size $512 \times 22 \times 5$. The coupled matrix is derived by stack the temperature records in a similar way, which results in a matrix of size 22×5 . We randomly choose 50% entries from the tensor and the matrix independently. For each algorithm we conduct 10 experiments for avoiding accident.

Fig. 5 reports the completion result. It can be seen that the proposed CTTC generates the lowest RMSE for both the spectrum tensor and the temperature matrix when TR rank is 2. The performance deteriorates when the TR rank becomes larger, which may implies the overfitting problem [37]. The individual TR completion method performs worse than the coupled one, which indicates the effectiveness of our method.

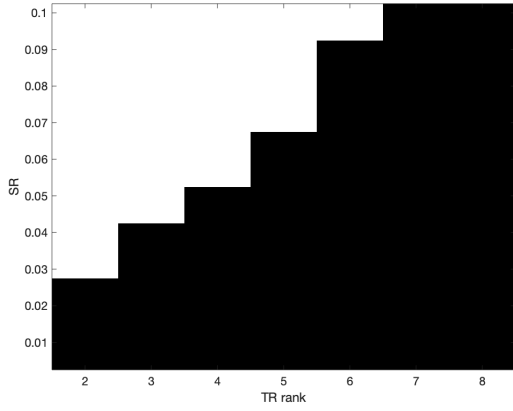
D. The Visual/Infrared Images

The dataset called "Reek" [47] is used in this section's experiment, which consists of a visual image and its infrared copy. This dataset is shown in Fig. 6, where the left figure is a RGB image and the right one is an infrared image. Both of them are compressed with resolution 240×320 since the original size is too large to conduct the experiment. We randomly select 50% entries from each image and run each algorithm 10 times independently for assuring fairness.

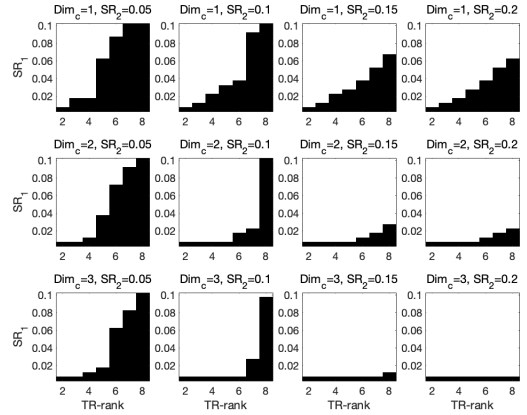
It can be seen from Fig. 7 that the CTTC yields lower RMSE than other coupled completion methods, though the uncoupled completion method produces a same RMSE, which demonstrates the lack of latent coupled structure of this dataset.

V. CONCLUSION

This paper investigates the coupled tensor completion via tensor ring decomposition and propose a non-convex algorithm which can be fast solved by alternating minimization. We also provides an excess risk bound which implies the sampling complexity can be reduced to below the theoretical bound. The proposed method assumes a strongly coupled relationship

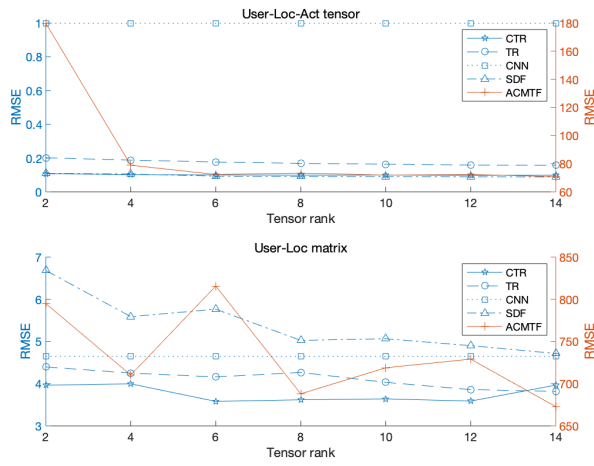


(a) The phase transition of an individual completion.

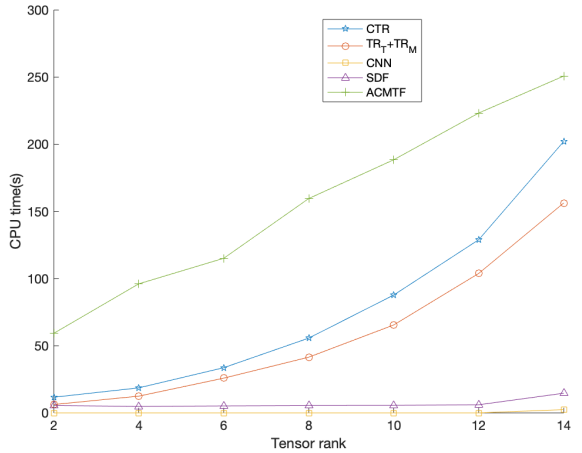


(b) The phase transition on TR rank versus sampling rate of tensor \mathcal{T}_1 with various sampling rates of tensor \mathcal{T}_2 and the numbers of coupled TR factors.

Fig. 3: The exact recovery result of randomly generated data with random sampling.

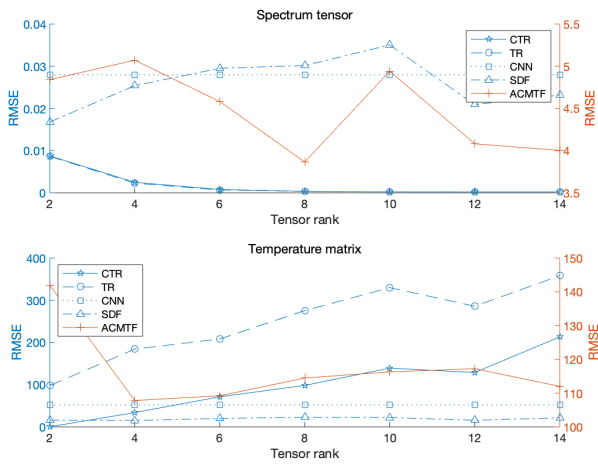


(a) RMSE

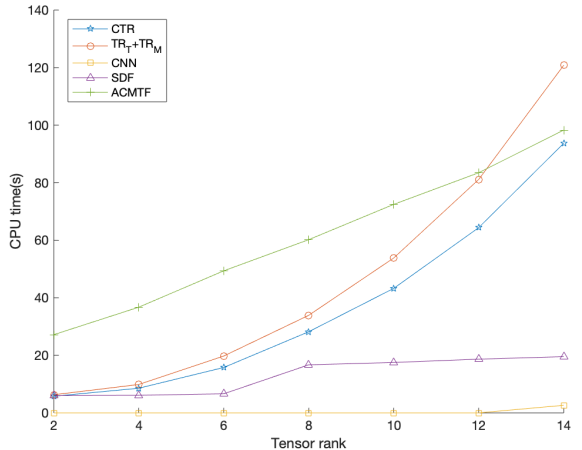


(b) CPU time (s)

Fig. 4: The completion result of the UCLAF data derived by five algorithms. The panel (a) is the RMSE comparison and the panel (b) is the elapsed CPU time.



(a) RMSE



(b) CPU time (s)

Fig. 5: The completion result of the SW-NIR data derived by five algorithms. The panel (a) is the RMSE comparison and the panel (b) is the elapsed CPU time.



Fig. 6: Display of the Reek data. The left figure is the RGB image and the right one is its infrared observation.

which may be strict for practical application. The experiments show that the coupled tensor ring structure can improve the completion performance.

APPENDIX A

OPTIMIZATION ON COUPLED TR FACTORS OF \mathfrak{R}_1 AND \mathfrak{R}_2

To solve problem (13), we calculate the second-order partial derivatives of the objective function with respect to $\alpha_{i_d}^{(d)}$, $\beta_{i_d}^{(d)}$, $\gamma_{i_d}^{(d)}$, respectively. We write the objective function as

$$\begin{aligned} f_{i_d}^{(d)} = & \frac{1}{2} \left[\alpha_{i_d}^{(d)}, \beta_{i_d}^{(d)} \right] \tilde{\mathbf{H}}_{i_d}^{(d)} \left[\alpha_{i_d}^{(d)}, \beta_{i_d}^{(d)} \right]^T - \\ & \left[\alpha_{i_d}^{(d)}, \beta_{i_d}^{(d)} \right] \mathbf{P}_d^T \bar{\mathbf{B}}_d \bar{\mathbf{c}}_{i_d}^{(d)T} + \frac{1}{2} \bar{\mathbf{c}}_{i_d}^{(d)} \bar{\mathbf{c}}_{i_d}^{(d)T} + \\ & \frac{1}{2} \left[\alpha_{i_d}^{(d)}, \gamma_{i_d}^{(d)} \right] \tilde{\mathbf{H}}_{i_d}^{\prime(d)} \left[\alpha_{i_d}^{(d)}, \gamma_{i_d}^{(d)} \right]^T - \\ & \left[\alpha_{i_d}^{(d)}, \gamma_{i_d}^{(d)} \right] \mathbf{P}_d^{\prime T} \bar{\mathbf{B}}_d^{\prime} \bar{\mathbf{c}}_{i_d}^{\prime(d)T} + \frac{1}{2} \bar{\mathbf{c}}_{i_d}^{\prime(d)} \bar{\mathbf{c}}_{i_d}^{\prime(d)T}, \end{aligned}$$

then there is

$$\begin{aligned} & \frac{\partial f_{i_d}^{(d)}}{\partial \alpha_{i_d}^{(d)}} \\ = & \frac{\partial}{\partial \alpha_{i_d}^{(d)}} \left\{ \frac{1}{2} \alpha_{i_d}^{(d)} \left(\tilde{\mathbf{H}}_{i_d}^{(d)11} + \tilde{\mathbf{H}}_{i_d}^{\prime(d)11} \right) \alpha_{i_d}^{(d)T} + \right. \\ & \alpha_{i_d}^{(d)} \left[\beta_{i_d}^{(d)} \left(\tilde{\mathbf{H}}_{i_d}^{(d)21} + \tilde{\mathbf{H}}_{i_d}^{(d)12T} \right) + \gamma_{i_d}^{(d)} \left(\tilde{\mathbf{H}}_{i_d}^{\prime(d)21} + \right. \right. \\ & \left. \left. \tilde{\mathbf{H}}_{i_d}^{\prime(d)12T} \right) + \xi_{i_d}^{(d)} + \xi_{i_d}^{\prime(d)} \right]^T + \frac{1}{2} \beta_{i_d}^{(d)} \tilde{\mathbf{H}}_{i_d}^{(d)22} \beta_{i_d}^{(d)T} + \\ & \frac{1}{2} \gamma_{i_d}^{(d)} \tilde{\mathbf{H}}_{i_d}^{\prime(d)22} \gamma_{i_d}^{(d)T} + \beta_{i_d}^{(d)} \eta_{i_d}^{(d)T} + \gamma_{i_d}^{(d)} \eta_{i_d}^{\prime(d)T} + \\ & \left. \frac{1}{2} z_{i_d}^{(d)} + \frac{1}{2} z_{i_d}^{\prime(d)} \right\} \\ = & \alpha_{i_d}^{(d)} \left(\tilde{\mathbf{H}}_{i_d}^{(d)11} + \tilde{\mathbf{H}}_{i_d}^{\prime(d)11} \right) + \varrho_{i_d}^{(d)}, \end{aligned}$$

where

$$\begin{aligned} & \varrho_{i_d}^{(d)} \\ = & \beta_{i_d}^{(d)} \left(\tilde{\mathbf{H}}_{i_d}^{(d)21} + \tilde{\mathbf{H}}_{i_d}^{(d)12T} \right) + \gamma_{i_d}^{(d)} \left(\tilde{\mathbf{H}}_{i_d}^{\prime(d)21} + \tilde{\mathbf{H}}_{i_d}^{\prime(d)12T} \right) \\ & + \xi_{i_d}^{(d)} + \xi_{i_d}^{\prime(d)}. \end{aligned}$$

Thus we have

$$\begin{cases} \frac{\partial^2 f_{i_d}^{(d)}}{\partial \alpha_{i_d}^{(d)2}} = \tilde{\mathbf{H}}_{i_d}^{(d)11} + \tilde{\mathbf{H}}_{i_d}^{\prime(d)11} \\ \frac{\partial^2 f_{i_d}^{(d)}}{\partial \alpha_{i_d}^{(d)} \partial \beta_{i_d}^{(d)}} = \tilde{\mathbf{H}}_{i_d}^{(d)12} + \tilde{\mathbf{H}}_{i_d}^{(d)21T} \\ \frac{\partial^2 f_{i_d}^{(d)}}{\partial \alpha_{i_d}^{(d)} \partial \gamma_{i_d}^{(d)}} = \tilde{\mathbf{H}}_{i_d}^{\prime(d)12} + \tilde{\mathbf{H}}_{i_d}^{\prime(d)21T} \end{cases}. \quad (18)$$

Then we deduce

$$\begin{aligned} \frac{\partial f_{i_d}^{(d)}}{\partial \beta_{i_d}^{(d)}} = & \frac{\partial}{\partial \beta_{i_d}^{(d)}} \left\{ \frac{1}{2} \beta_{i_d}^{(d)} \tilde{\mathbf{H}}_{i_d}^{(d)22} \beta_{i_d}^{(d)T} + \beta_{i_d}^{(d)} \left[\alpha_{i_d}^{(d)} \left(\tilde{\mathbf{H}}_{i_d}^{(d)12} \right. \right. \right. \\ & \left. \left. + \tilde{\mathbf{H}}_{i_d}^{(d)21T} \right) + \eta_{i_d}^{(d)} \right]^T + \frac{1}{2} \gamma_{i_d}^{(d)} \tilde{\mathbf{H}}_{i_d}^{\prime(d)22} \gamma_{i_d}^{(d)T} + \\ & \gamma_{i_d}^{(d)} \left[\alpha_{i_d}^{(d)} \left(\tilde{\mathbf{H}}_{i_d}^{\prime(d)12} + \tilde{\mathbf{H}}_{i_d}^{\prime(d)21T} \right) + \eta_{i_d}^{\prime(d)} \right]^T + \\ & \frac{1}{2} \alpha_{i_d}^{(d)} \left(\tilde{\mathbf{H}}_{i_d}^{(d)11} + \tilde{\mathbf{H}}_{i_d}^{\prime(d)11} \right) \alpha_{i_d}^{(d)T} + \\ & \left. \alpha_{i_d}^{(d)} \left(\xi_{i_d}^{(d)} + \xi_{i_d}^{\prime(d)} \right)^T + \frac{1}{2} z_{i_d}^{(d)} + \frac{1}{2} z_{i_d}^{\prime(d)} \right\} \\ = & \beta_{i_d}^{(d)} \tilde{\mathbf{H}}_{i_d}^{(d)22} + \vartheta_{i_d}^{(d)}, \end{aligned}$$

where $\vartheta_{i_d}^{(d)} = \alpha_{i_d}^{(d)} \left(\tilde{\mathbf{H}}_{i_d}^{(d)12} + \tilde{\mathbf{H}}_{i_d}^{(d)21T} \right) + \eta_{i_d}^{(d)}$. Hence there is

$$\begin{cases} \frac{\partial^2 f_{i_d}^{(d)}}{\partial \beta_{i_d}^{(d)2}} = \tilde{\mathbf{H}}_{i_d}^{(d)22}, \quad \frac{\partial^2 f_{i_d}^{(d)}}{\partial \beta_{i_d}^{(d)} \partial \alpha_{i_d}^{(d)}} = \tilde{\mathbf{H}}_{i_d}^{(d)21} + \tilde{\mathbf{H}}_{i_d}^{(d)12T} \\ \frac{\partial^2 f_{i_d}^{(d)}}{\partial \beta_{i_d}^{(d)} \partial \gamma_{i_d}^{(d)}} = \mathbf{0} \end{cases}. \quad (19)$$

Similarly, we derive

$$\begin{cases} \frac{\partial^2 f_{i_d}^{(d)}}{\partial \gamma_{i_d}^{(d)2}} = \tilde{\mathbf{H}}_{i_d}^{\prime(d)22}, \quad \frac{\partial^2 f_{i_d}^{(d)}}{\partial \gamma_{i_d}^{(d)} \partial \alpha_{i_d}^{(d)}} = \tilde{\mathbf{H}}_{i_d}^{\prime(d)21} + \tilde{\mathbf{H}}_{i_d}^{\prime(d)12T} \\ \frac{\partial^2 f_{i_d}^{(d)}}{\partial \gamma_{i_d}^{(d)} \partial \beta_{i_d}^{(d)}} = \mathbf{0} \end{cases}. \quad (20)$$

Incorporating (18) – (20), we derive the Hessian matrix

$$\hat{\mathbf{H}}_{i_d} = \begin{bmatrix} \tilde{\mathbf{H}}_{i_d}^{(d)11} + \tilde{\mathbf{H}}_{i_d}^{\prime(d)11} & \tilde{\mathbf{H}}_{i_d}^{(d)12} + \tilde{\mathbf{H}}_{i_d}^{(d)21T} & \tilde{\mathbf{H}}_{i_d}^{\prime(d)12} + \tilde{\mathbf{H}}_{i_d}^{\prime(d)21T} \\ \tilde{\mathbf{H}}_{i_d}^{(d)21} + \tilde{\mathbf{H}}_{i_d}^{(d)12T} & \tilde{\mathbf{H}}_{i_d}^{(d)22} & \mathbf{0} \\ \tilde{\mathbf{H}}_{i_d}^{\prime(d)21} + \tilde{\mathbf{H}}_{i_d}^{\prime(d)12T} & \mathbf{0} & \tilde{\mathbf{H}}_{i_d}^{\prime(d)22} \end{bmatrix}.$$

APPENDIX B

PROOF OF THEOREM 1

A. The expectation of a linear combination of products of independent variables

Supposing X_i , $i = 1, \dots, m$ and Y_j , $j = 1, \dots, n$ are the independent Gamma variables with a same shape parameter $k/2$ and a scale parameter 2σ , where σ is the standard deviation of all elements of each TR factor. It follows that the density function of X_i is $p(x_i) = x_i^{k/2-1} \exp(-x_i/2\sigma) / (2\sigma)^{k/2} \Gamma(k/2)$, where $\Gamma(\cdot)$ is the

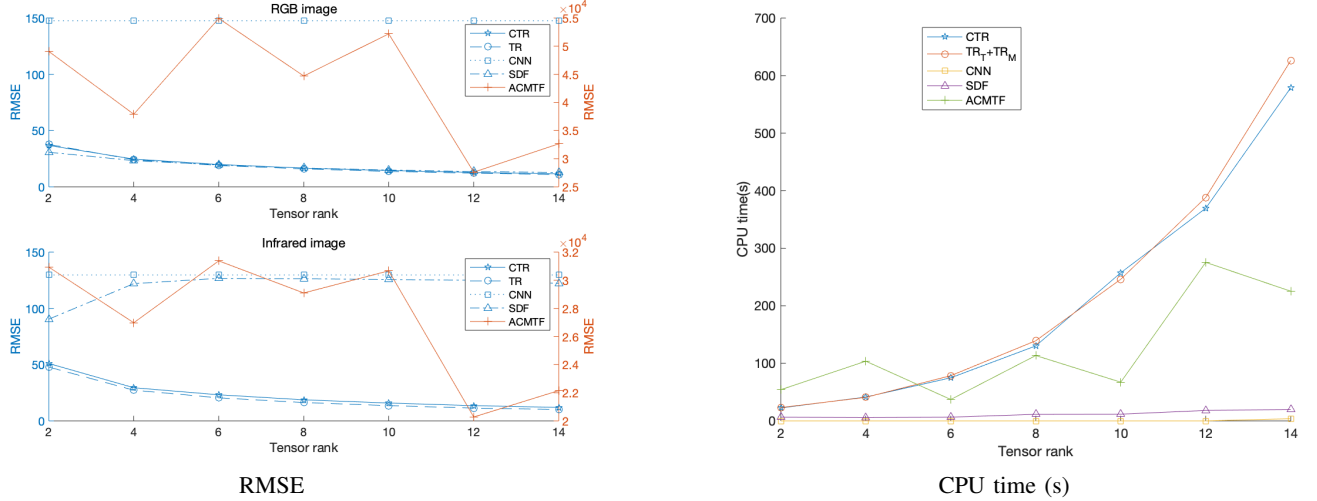


Fig. 7: The completion result of the SW-NIR data derived by five algorithms. The panel (a) is the RMSE comparison and the panel (b) is the elapsed CPU time.

Gamma function. We assume $0 < \alpha < 1$ and $0 < \beta < 1$, then the expectation of $\sqrt{\alpha \prod_{i=1}^m X_i + \beta \prod_{j=1}^n Y_j}$ is given by the multiple integral

$$\int_0^{+\infty} \cdots \int_0^{+\infty} \sqrt{\alpha \prod_{i=1}^m x_i + \beta \prod_{j=1}^n y_j} \prod_{i=1}^m p(x_i) \prod_{j=1}^n p(y_j) dx_1 \cdots dx_m dy_1 \cdots dy_n.$$

The calculation of this integral is done with the help of the method of brackets, which expands a definite integral evaluating over the half line $[0, +\infty)$ as a series consisting of the brackets. For example, the notation $\langle a \rangle$ stands for the divergent integral $\int_0^{+\infty} x^{a-1} dx$. The indicator $\phi_n \triangleq (-1)^n / \Gamma(n+1)$ will be used in the series expressions when applying the method of brackets. The Pochhammer symbols defined as $(b)_n \triangleq \Gamma(n+b) / \Gamma(b)$ is a systematic procedure in the simplification of the series. An exponential function $\exp(-x)$ can be represented as $\sum_n \phi_n x^n$ in the framework of the method of brackets. Another useful rule is that a multinomial $(x_1 + \cdots + x_m)^a$ is expanded as $\sum_{\{n\}} \phi_{\{n\}} x_1^{n_1} \cdots x_m^{n_m} \langle n_1 + \cdots + n_m - a \rangle / \Gamma(-a)$.

We start with the two rules, slinging out the terms that do not contain the integral variables, merging the remained terms and substituting the integral with brackets, the integral is transformed into

$$\frac{(2\sigma)^{-\frac{(m+n)k}{2}}}{\Gamma(-\frac{1}{2}) \Gamma^{m+n}(\frac{k}{2})} \sum_{w_1, w_2=0}^{+\infty} \phi_{w_1 w_2} \alpha^{w_1} \beta^{w_2} \langle w_1 + w_2 - \frac{1}{2} \rangle \prod_{i=1}^m \prod_{j=1}^n \sum_{p_i} \sum_{q_j} \frac{\phi_{p_i q_j}}{(2\sigma)^{p_i + q_j}} \langle p_i + w_1 + \frac{k}{2} \rangle \langle q_j + w_2 + \frac{k}{2} \rangle.$$

To continue, we choose w_1 and w_2 as free variables and eliminate the other brackets. The result shown below follows from the rule that the value assigned to $\sum_n \phi_n f(n) \langle cn+d \rangle$ is $f(n^*) \Gamma(-n^*) / |c|$, where n^* is obtained from the vanishing

of the bracket.

$$\frac{1}{\Gamma(-\frac{1}{2}) \Gamma^{m+n}(\frac{k}{2})} \sum_{w_1, w_2=0}^{+\infty} \phi_{w_1 w_2} [\alpha (2\sigma)^m]^{w_1} [\beta (2\sigma)^n]^{w_2} \Gamma^m\left(w_1 + \frac{k}{2}\right) \Gamma^n\left(w_2 + \frac{k}{2}\right) \langle w_1 + w_2 - \frac{1}{2} \rangle$$

The matrix of coefficients left has rank 1, thus it produces two series as candidates for the values of the integral, one per free variable. The simplified formulation derives from the Pochhammer symbols and the transformation $(b)_{-n} = (-1)^n / (1-b)_n$ which can be proved by repeatedly using the recurrence relation $\Gamma(x) = \Gamma(x+1)/x = (x-1)\Gamma(x-1)$. The final result is obtained by introducing the hypergeometric function ${}_pF_q(\cdots|\cdot)$.

1) Case 1: The variable w_1 is free. Thus Plugging $w_2^* = 1/2 - w_1$ into the rule gives

$$T_1 = \sqrt{\beta (2\sigma)^n} \frac{\Gamma^n(\frac{k+1}{2})}{\Gamma^n(\frac{k}{2})} {}_{m+1}F_n \left(\begin{matrix} -\frac{1}{2}, \frac{k}{2}, \dots, \frac{k}{2} \\ \frac{1-k}{2}, \dots, \frac{1-k}{2} \end{matrix} \middle| \frac{(-1)^{n+1} \alpha (2\sigma)^m}{\beta (2\sigma)^n} \right).$$

2) Case 2: The variable w_2 is free. Then Plugging $w_1^* = 1/2 - w_2$ into the rule yields

$$T_2 = \sqrt{\alpha (2\sigma)^m} \frac{\Gamma^m(\frac{k+1}{2})}{\Gamma^m(\frac{k}{2})} {}_{n+1}F_m \left(\begin{matrix} -\frac{1}{2}, \frac{k}{2}, \dots, \frac{k}{2} \\ \frac{1-k}{2}, \dots, \frac{1-k}{2} \end{matrix} \middle| \frac{(-1)^{m+1} \beta (2\sigma)^n}{\alpha (2\sigma)^m} \right).$$

Which of the two expressions is used depends on the convergence condition of the hypergeometric function. The first one is employed if $n \geq m$, otherwise the second one is considered.

B. Bounding the expectation of the F-norm of two coupled tensors

Without loss of generality, supposing \mathcal{X} and \mathcal{Y} are D_1 -order and D_2 -order tensors coupled on their first L modes,

with a same TR rank and a dimensional size. To calculate $\mathbb{E}\sqrt{\alpha\|\mathcal{X}\|_F^2 + \beta\|\mathcal{Y}\|_F^2}$, we first note that $\|\cdot\|_F$ is submultiplicative, thus

$$\begin{aligned} & \mathbb{E}\sqrt{\alpha\|\mathcal{X}\|_F^2 + \beta\|\mathcal{Y}\|_F^2} \\ & \leq \mathbb{E}\prod_{l=1}^L \|\mathcal{U}^{(l)}\|_F \sqrt{\alpha \prod_{d_1=L+1}^{D_1} \|\mathcal{U}^{(d_1)}\|_F^2 + \beta \prod_{d_2=L+1}^{D_2} \|\mathcal{V}^{(d_2)}\|_F^2} \\ & = \sqrt{\alpha} (2\sigma)^{\frac{D_1}{2}} \frac{\Gamma^{D_1}(\frac{k+1}{2})}{\Gamma^{D_1}(\frac{k}{2})} \\ & \quad D_{2+1-L} F_{D_1-L} \left(\begin{matrix} -\frac{1}{2}, \frac{k}{2}, \dots, \frac{k}{2} \\ \frac{1-k}{2}, \dots, \frac{1-k}{2} \end{matrix} \middle| (-1)^{D_1+1-L} \frac{\beta (2\sigma)^{D_2}}{\alpha (2\sigma)^{D_1}} \right) \end{aligned} \quad (21)$$

holds for $D_1 \geq D_2$ and

$$\begin{aligned} & \mathbb{E}\sqrt{\alpha\|\mathcal{X}\|_F^2 + \beta\|\mathcal{Y}\|_F^2} \\ & \leq \sqrt{\beta} (2\sigma)^{\frac{D_2}{2}} \frac{\Gamma^{D_2}(\frac{k+1}{2})}{\Gamma^{D_2}(\frac{k}{2})} \\ & \quad D_{1+1-L} F_{D_2-L} \left(\begin{matrix} -\frac{1}{2}, \frac{k}{2}, \dots, \frac{k}{2} \\ \frac{1-k}{2}, \dots, \frac{1-k}{2} \end{matrix} \middle| (-1)^{D_2+1-L} \frac{\alpha (2\sigma)^{D_1}}{\beta (2\sigma)^{D_2}} \right) \end{aligned} \quad (22)$$

holds for $D_2 \geq D_1$.

C. Bounding the excess risk

A subset \mathbf{x}_{m_1} containing $m_1 = |\mathbb{S}_1 \cup \mathbb{T}_1|$ elements is sampled uniformly without replacement from $\text{vec}(\mathcal{X})$. We concatenate \mathbf{x}_{m_1} and \mathbf{y}_{m_2} as a vector $\mathbf{z}_m \triangleq [\mathbf{x}_{m_1}; \mathbf{y}_{m_2}]$ where $m = |\mathbb{S} \cup \mathbb{T}|$.

where

$$\hat{Q}_{m,n}(\bar{l}_{\mathbb{T}}, \mathbf{z}_m) = \mathbb{E}_{\mathbf{z}_n} \left[\sup_{\mathcal{X}, \mathcal{Y} \in \mathcal{H}} \bar{l}_{\mathbb{T}}(\mathbf{z}_k, \mathbf{t}_k) - \bar{l}_{\mathbb{T}}(\mathbf{z}_n, \mathbf{t}_n) \right],$$

where \mathbf{z}_n , $n \in \{1, \dots, m-1\}$ is a random subset of \mathbf{z}_m containing n elements sampled uniformly without replacement and $\mathbf{z}_k \triangleq \mathbf{z}_m \setminus \mathbf{z}_n$.

Under the hypothesis \mathcal{H} mentioned before, let $m = 2n = |\mathbb{T}_1 \cup \mathbb{T}_2|$, then the expectation of the permutational

Rademacher complexity is bounded as

$$\begin{aligned} & \mathbb{E}_{\mathbf{z}_m} \left[\hat{Q}_{m,m/2}(\bar{l}_{\mathbb{T}}, \mathbf{z}_m) \right] \\ & \leq \mathbb{E}_{\mathbf{z}_m} \left\{ \left(1 + \frac{2}{\sqrt{2\pi|\mathbb{T}|-2}} \right) \mathbb{E}_{\varepsilon} \left[\sup_{\mathcal{X}, \mathcal{Y} \in \mathcal{H}} \frac{2}{|\mathbb{T}|} \varepsilon^T \bar{l}_{\mathbb{T}}(\mathbf{z}_m, \mathbf{t}_m) \right] \right\} \\ & \leq \mathbb{E}_{\mathbf{z}_m} \left\{ \Lambda \left(1 + \frac{2}{\sqrt{2\pi|\mathbb{T}|-2}} \right) \frac{2}{|\mathbb{T}|} \mathbb{E}_{\varepsilon} \left[\sup_{\mathcal{X}, \mathcal{Y} \in \mathcal{H}} \varepsilon^T \mathbf{z}_m \right] \right\} \\ & \leq \Lambda \left(1 + \frac{2}{\sqrt{2\pi|\mathbb{T}|-2}} \right) \frac{2}{|\mathbb{T}|} \mathbb{E}_{\varepsilon, \mathbf{z}_m} \left[\sup_{\mathcal{X}, \mathcal{Y} \in \mathcal{H}} \|\varepsilon\|_F \|\mathbf{z}_m\|_F \right] \\ & = \Lambda \left(1 + \frac{2}{\sqrt{2\pi|\mathbb{T}|-2}} \right) \frac{2}{\sqrt{|\mathbb{T}|}} \mathbb{E}_{\mathbf{z}_m} \left[\sup_{\mathcal{X}, \mathcal{Y} \in \mathcal{H}} \|\mathbf{z}_m\|_F \right] \\ & = \Lambda \left(1 + \frac{2}{\sqrt{2\pi|\mathbb{T}|-2}} \right) \frac{2}{\sqrt{|\mathbb{T}|}} \frac{\mathbb{E}}{m+1} \sum_{i=0}^m \frac{1}{\binom{|\mathbb{T}_1 \cup \mathbb{S}_1|}{i} \binom{|\mathbb{T}_2 \cup \mathbb{S}_2|}{m-i}} \\ & \quad \sum_{\mathbf{z}_m^{(1)} \subseteq \mathbb{T}_1 \cup \mathbb{S}_1} \sum_{\mathbf{z}_m^{(2)} \subseteq \mathbb{T}_2 \cup \mathbb{S}_2} \sqrt{\sum_{x_j \in \mathbf{z}_m^{(1)}} x_j^2 + \sum_{y_j \in \mathbf{z}_m^{(2)}} y_j^2} \\ & \leq \Lambda \left(1 + \frac{2}{\sqrt{2\pi|\mathbb{T}|-2}} \right) \frac{2}{\sqrt{|\mathbb{T}|}} \frac{1}{m+1} \\ & \quad \mathbb{E} \sum_{i=0}^m \sqrt{\frac{\binom{|\mathbb{T}_1 \cup \mathbb{S}_1|-1}{i-1}}{\binom{|\mathbb{T}_1 \cup \mathbb{S}_1|}{i}} \|\mathbf{x}_{\mathbb{T}_1 \cup \mathbb{S}_1}\|_2^2 + \frac{\binom{|\mathbb{T}_2 \cup \mathbb{S}_2|-1}{m-i-1}}{\binom{|\mathbb{T}_2 \cup \mathbb{S}_2|}{m-i}} \|\mathbf{y}_{\mathbb{T}_2 \cup \mathbb{S}_2}\|_2^2} \\ & = \sqrt{2} \Lambda \left(1 + \frac{2}{\sqrt{2\pi|\mathbb{T}|-2}} \right) \mathbb{E} \sqrt{\frac{\|\mathbf{x}_{\mathbb{T}_1 \cup \mathbb{S}_1}\|_2^2}{|\mathbb{T}_1 \cup \mathbb{S}_1|} + \frac{\|\mathbf{y}_{\mathbb{T}_2 \cup \mathbb{S}_2}\|_2^2}{|\mathbb{T}_2 \cup \mathbb{S}_2|}} \\ & \leq \Lambda \left(1 + \frac{2}{\sqrt{2\pi|\mathbb{T}|-2}} \right) \mathbb{E} \sqrt{\frac{\|\mathcal{X}\|_F^2}{|\mathbb{T}_1|} + \frac{\|\mathcal{Y}\|_F^2}{|\mathbb{T}_2|}}, \end{aligned}$$

where the first inequality follows from the Theorem 3 in [44], the second inequality is a result of Rademacher contraction, the third inequality comes from the Hlder's inequality, the fourth inequality is a consequence of arithmetic mean-quadratic mean inequality. Due to the hypothesis \mathcal{H} , the final bounds can be derived by plugging (21) and (22) with $\alpha = 1/|\mathbb{T}_1|$ and $\beta = 1/|\mathbb{T}_2|$.

REFERENCES

- [1] A. Cichocki, "Era of big data processing: a new approach via tensor networks and tensor decompositions," *arXiv preprint arXiv:1403.2048*, 2014.
- [2] A. Cichocki, D. Mandic, L. De Lathauwer, G. Zhou, Q. Zhao, C. Caiafa, and H. A. Phan, "Tensor decompositions for signal processing applications: from two-way to multiway component analysis," *IEEE Signal Processing Magazine*, vol. 32, no. 2, pp. 145–163, 2015.
- [3] A. Cichocki, N. Lee, I. Oseledets, A.-H. Phan, Q. Zhao, D. P. Mandic, *et al.*, "Tensor networks for dimensionality reduction and large-scale optimization: part 1 low-rank tensor decompositions," *Foundations and Trends® in Machine Learning*, vol. 9, no. 4-5, pp. 249–429, 2016.
- [4] A. Cichocki, A.-H. Phan, Q. Zhao, N. Lee, I. Oseledets, M. Sugiyama, D. P. Mandic, *et al.*, "Tensor networks for dimensionality reduction and large-scale optimization: Part 2 applications and future perspectives," *Foundations and Trends® in Machine Learning*, vol. 9, no. 6, pp. 431–673, 2017.
- [5] N. D. Sidiropoulos, L. De Lathauwer, X. Fu, K. Huang, E. E. Papalexakis, and C. Faloutsos, "Tensor decomposition for signal processing and machine learning," *IEEE Transactions on Signal Processing*, vol. 65, no. 13, pp. 3551–3582, 2017.

- [6] Y. Liu, F. Shang, H. Cheng, J. Cheng, and H. Tong, "Factor matrix trace norm minimization for low-rank tensor completion," in *Proceedings of the 2014 SIAM International Conference on Data Mining*, pp. 866–874, SIAM, 2014.
- [7] D. M. Dunlavy, T. G. Kolda, and E. Acar, "Temporal link prediction using matrix and tensor factorizations," *ACM Transactions on Knowledge Discovery from Data (TKDD)*, vol. 5, no. 2, p. 10, 2011.
- [8] B. Ermiş, E. Acar, and A. T. Cemgil, "Link prediction in heterogeneous data via generalized coupled tensor factorization," *Data Mining and Knowledge Discovery*, vol. 29, no. 1, pp. 203–236, 2015.
- [9] P. Symeonidis, "Matrix and tensor decomposition in recommender systems," in *Proceedings of the 10th ACM Conference on Recommender Systems*, pp. 429–430, ACM, 2016.
- [10] S. Rendle, "Factorization machines," in *2010 IEEE International Conference on Data Mining*, pp. 995–1000, IEEE, 2010.
- [11] S. Rendle and L. Schmidt-Thieme, "Pairwise interaction tensor factorization for personalized tag recommendation," in *Proceedings of the third ACM international conference on Web search and data mining*, pp. 81–90, ACM, 2010.
- [12] J. Peng, D. D. Zeng, H. Zhao, and F.-y. Wang, "Collaborative filtering in social tagging systems based on joint item-tag recommendations," in *Proceedings of the 19th ACM international conference on Information and knowledge management*, pp. 809–818, ACM, 2010.
- [13] L. Xiong, X. Chen, T.-K. Huang, J. Schneider, and J. G. Carbonell, "Temporal collaborative filtering with bayesian probabilistic tensor factorization," in *Proceedings of the 2010 SIAM international conference on data mining*, pp. 211–222, SIAM, 2010.
- [14] A. Karatzoglou, X. Amatriain, L. Baltrunas, and N. Oliver, "Multiverse recommendation: n-dimensional tensor factorization for context-aware collaborative filtering," in *Proceedings of the fourth ACM conference on Recommender systems*, pp. 79–86, ACM, 2010.
- [15] S. Gandy, B. Recht, and I. Yamada, "Tensor completion and low-n-rank tensor recovery via convex optimization," *Inverse Problems*, vol. 27, no. 2, p. 025010, 2011.
- [16] J. A. Bazerque, G. Mateos, and G. B. Giannakis, "Rank regularization and bayesian inference for tensor completion and extrapolation," *IEEE transactions on signal processing*, vol. 61, no. 22, pp. 5689–5703, 2013.
- [17] Y. Liu, F. Shang, L. Jiao, J. Cheng, and H. Cheng, "Trace norm regularized candecomp/parafac decomposition with missing data," *IEEE transactions on cybernetics*, vol. 45, no. 11, pp. 2437–2448, 2014.
- [18] J. Dauwels, L. Garg, A. Earnest, and L. K. Pang, "Handling missing data in medical questionnaires using tensor decompositions," in *2011 8th International Conference on Information, Communications & Signal Processing*, pp. 1–5, IEEE, 2011.
- [19] E. Acar, D. M. Dunlavy, T. G. Kolda, and M. Mørup, "Scalable tensor factorizations for incomplete data," *Chemometrics and Intelligent Laboratory Systems*, vol. 106, no. 1, pp. 41–56, 2011.
- [20] A. Narita, K. Hayashi, R. Tomioka, and H. Kashima, "Tensor factorization using auxiliary information," *Data Mining and Knowledge Discovery*, vol. 25, no. 2, pp. 298–324, 2012.
- [21] W. Chu and Z. Ghahramani, "Probabilistic models for incomplete multidimensional arrays," in *Artificial Intelligence and Statistics*, pp. 89–96, 2009.
- [22] M. Signoretto, R. Van de Plas, B. De Moor, and J. A. Suykens, "Tensor versus matrix completion: a comparison with application to spectral data," *IEEE Signal Processing Letters*, vol. 18, no. 7, pp. 403–406, 2011.
- [23] M. F. Duarte and R. G. Baraniuk, "Kronecker compressive sensing," *IEEE Transactions on Image Processing*, vol. 21, no. 2, pp. 494–504, 2011.
- [24] J. Liu, P. Musialski, P. Wonka, and J. Ye, "Tensor completion for estimating missing values in visual data," *IEEE Transactions on Pattern Analysis and Machine Intelligence*, vol. 35, no. 1, pp. 208–220, 2013.
- [25] J. Liu, P. Musialski, P. Wonka, and J. Ye, "Tensor completion for estimating missing values in visual data," *IEEE transactions on pattern analysis and machine intelligence*, vol. 35, no. 1, pp. 208–220, 2012.
- [26] M. E. Kilmer, K. Braman, N. Hao, and R. C. Hoover, "Third-order tensors as operators on matrices: a theoretical and computational framework with applications in imaging," *SIAM Journal on Matrix Analysis and Applications*, vol. 34, no. 1, pp. 148–172, 2013.
- [27] C. Mu, B. Huang, J. Wright, and D. Goldfarb, "Square deal: Lower bounds and improved relaxations for tensor recovery," in *International conference on machine learning*, pp. 73–81, 2014.
- [28] H. Kasai, "Online low-rank tensor subspace tracking from incomplete data by cp decomposition using recursive least squares," in *2016 IEEE International Conference on Acoustics, Speech and Signal Processing (ICASSP)*, pp. 2519–2523, IEEE, 2016.
- [29] W. Wang, Y. Sun, B. Eriksson, W. Wang, and V. Aggarwal, "Wide compression: Tensor ring nets," in *Proceedings of the IEEE Conference on Computer Vision and Pattern Recognition*, pp. 9329–9338, 2018.
- [30] W. He, L. Yuan, and N. Yokoya, "Total-variation-regularized tensor ring completion for remote sensing image reconstruction," in *ICASSP 2019-2019 IEEE International Conference on Acoustics, Speech and Signal Processing (ICASSP)*, pp. 8603–8607, IEEE, 2019.
- [31] H. Huang, Y. Liu, J. Liu, and C. Zhu, "Provable tensor ring completion," *Signal Processing*, vol. 171, p. 107486, 2020.
- [32] E. Acar, T. G. Kolda, and D. M. Dunlavy, "All-at-once optimization for coupled matrix and tensor factorizations," *arXiv preprint arXiv:1105.3422*, 2011.
- [33] E. Acar, A. J. Lawaetz, M. A. Rasmussen, and R. Bro, "Structure-revealing data fusion model with applications in metabolomics," in *2013 35th Annual International Conference of the IEEE Engineering in Medicine and Biology Society (EMBC)*, pp. 6023–6026, IEEE, 2013.
- [34] E. Acar, E. E. Papalexakis, G. Gürdeniz, M. A. Rasmussen, A. J. Lawaetz, M. Nilsson, and R. Bro, "Structure-revealing data fusion," *BMC bioinformatics*, vol. 15, no. 1, p. 239, 2014.
- [35] L. Sorber, M. Van Barel, and L. De Lathauwer, "Structured data fusion," *IEEE Journal of Selected Topics in Signal Processing*, vol. 9, no. 4, pp. 586–600, 2015.
- [36] J. A. Bengua, H. N. Phien, H. D. Tuan, and M. N. Do, "Efficient tensor completion for color image and video recovery: low-rank tensor train," *IEEE Transactions on Image Processing*, vol. 26, no. 5, pp. 2466–2479, 2017.
- [37] W. Wang, V. Aggarwal, and S. Aeron, "Efficient low rank tensor ring completion," in *Computer Vision (ICCV), 2017 IEEE International Conference on*, IEEE, 2017.
- [38] K. Wimalawarne and H. Mamitsuka, "Efficient convex completion of coupled tensors using coupled nuclear norms," in *Advances in Neural Information Processing Systems*, pp. 6902–6910, 2018.
- [39] R. Orús, "A practical introduction to tensor networks: Matrix product states and projected entangled pair states," *Annals of Physics*, vol. 349, pp. 117–158, 2014.
- [40] Q. Zhao, M. Sugiyama, and A. Cichocki, "Learning efficient tensor representations with ring structure networks," *arXiv preprint arXiv:1705.08286*, 2017.
- [41] I. V. Oseledets, "Tensor-train decomposition," *SIAM Journal on Scientific Computing*, vol. 33, no. 5, pp. 2295–2317, 2011.
- [42] Y. Xu, Z. Wu, J. Chanussot, and Z. Wei, "Hyperspectral images super-resolution via learning high-order coupled tensor ring representation," *IEEE Transactions on Neural Networks and Learning Systems*, 2020.
- [43] Y. Xu and W. Yin, "A block coordinate descent method for regularized multiconvex optimization with applications to nonnegative tensor factorization and completion," *SIAM Journal on Imaging Sciences*, vol. 6, no. 3, pp. 1758–1789, 2013.
- [44] I. Tolstikhin, N. Zhivotovskiy, and G. Blanchard, "Permutational rademacher complexity," in *International Conference on Algorithmic Learning Theory*, pp. 209–223, Springer, 2015.
- [45] V. W. Zheng, B. Cao, Y. Zheng, X. Xie, and Q. Yang, "Collaborative filtering meets mobile recommendation: A user-centered approach," in *Twenty-Fourth AAAI Conference on Artificial Intelligence*, 2010.
- [46] F. Wülfert, W. T. Kok, and A. K. Smilde, "Influence of temperature on vibrational spectra and consequences for the predictive ability of multivariate models," *Analytical chemistry*, vol. 70, no. 9, pp. 1761–1767, 1998.
- [47] A. Toet, M. J. de Jong, M. A. Hogervorst, and I. T. Hooge, "Perceptual evaluation of color transformed multispectral imagery," *Optical Engineering*, vol. 53, no. 4, p. 043101, 2014.